A 3800 yr paleoseismic record (Lake Hazar sediments, eastern Turkey): Implications for the East Anatolian Fault seismic cycle

Aurélia Hubert-Ferrari [a,*], Laura Lamair [a], Sophie Hage [b], Sabine Schmidt [c], M. Namık Çağatay [d], Ulaş Avşar [e]

[a] *University of Liège, Department of Geography, clos Mercator 3, 4000, Liège, Belgium*
[b] *National Oceanography Centre Southampton, University of Southampton, UK*
[c] *EPOC, Université de Bordeaux, France*
[d] *Istanbul Teknik Universitesi, EMCOL Research Centre, İstanbul, Turkey*
[e] *Middle East Technical University, Faculty of Engineering, Geological Engineering, Ankara, Turkey*

ARTICLE INFO

ABSTRACT

The East Anatolian Fault (EAF) in Turkey is a major active left-lateral strike-slip fault that was seismically active during the 19th century but mostly quiet during the 20th century. Geodetic data suggests that the fault is creeping along its central part. Here we focus on its seismic history as recorded in the sediments of Lake Hazar in the central part of the EAF. Sediment cores were studied using X-ray imagery, magnetic susceptibility, grain-size, loss-on-ignition and X-ray fluorescence measurements. Recurring thin, coarse-grained sediment units identified as turbidites in all cores were deposited synchronously at two deep study sites. The turbidite ages are inferred combining radiocarbon and radionuclide (^{137}Cs and ^{210}Pb) dating in an Oxcal model. A mean recurrence interval of $\sim$190 yrs is obtained over 3800 yrs. Ages of the recent turbidites correspond to historical earthquakes reported to have occurred along the EAF Zone or to paleoruptures documented in trenches just northeast of Lake Hazar. The turbidites are inferred to be earthquake-triggered. Our record demonstrates that Lake Hazar has been repeatedly subjected to significant seismic shaking over the past 3800 yrs. The seismic sources are variable: $\sim$65% of all turbidites are associated with an EAF source. The seismic cycle of central EAF is thus only partly impacted by creep.

© 2020 Elsevier B.V. All rights reserved.

1. Introduction

Subaqueous paleoseismology allows retrieval of long-term earthquake records in areas inaccessible to classical paleoseismic investigations, along submarine faults, such as in the Marmara Sea area (e.g. Drab et al., 2012; 2015; Çağatay et al., 2012), or in the Gulf of Corinth (e.g. Beckers et al., 2017). Onland lacustrine archives have also been used as paleoseismometers capable of recording earthquake shaking (i.e. Strasser et al., 2013) and to complement classical paleoseismology, e.g. along the North Anatolian Fault (NAF) (Avşar et al., 2014a, 2014b).

The present study focuses on the East Anatolian Fault (EAF), a major strike-slip fault in Turkey that accommodates with its conjugate NAF, the westward block motion of the Anatolian Plate. The fault lacks paleoseismological data. Only two earthquakes of magnitude larger than 6 occurred during the 20th century. Yet, historical seismicity suggests that the fault is capable of generating earthquakes of magnitude greater than 7 (Ambraseys, 1989). This question is key to assess seismic hazard in the area. Large earthquake occurrence needs also to be reconciled with fault creep documented by InSAR (Cavalié and Jónsson, 2014). The present study addresses these issues by providing a long-term paleoseismic record extracted from Lake Hazar crossed by the central segment of the EAF.

Aims

We use Lake Hazar sediments to reconstruct the paleoseismic history of the EAF. Lake Hazar occupies an active tectonic basin. The area has sustained two major earthquakes in 1874 and 1875, whose sedimentological imprints were recently documented (Hubert-Ferrari et al., 2017). The deep lacustrine sediments show frequent thin turbidites. Their depositional process and composition have been studied and an earthquake trigger inferred in Hage et al. (2017). Here we obtain a long record of turbidites using short and long cores recovered from >70 m water depth. We build an age model combining short-lived radiogenic nuclides, radiocarbon dating and hemipelagic sediment thickness to constrain the turbidite history. We compare the turbidites found in Lake Hazar with
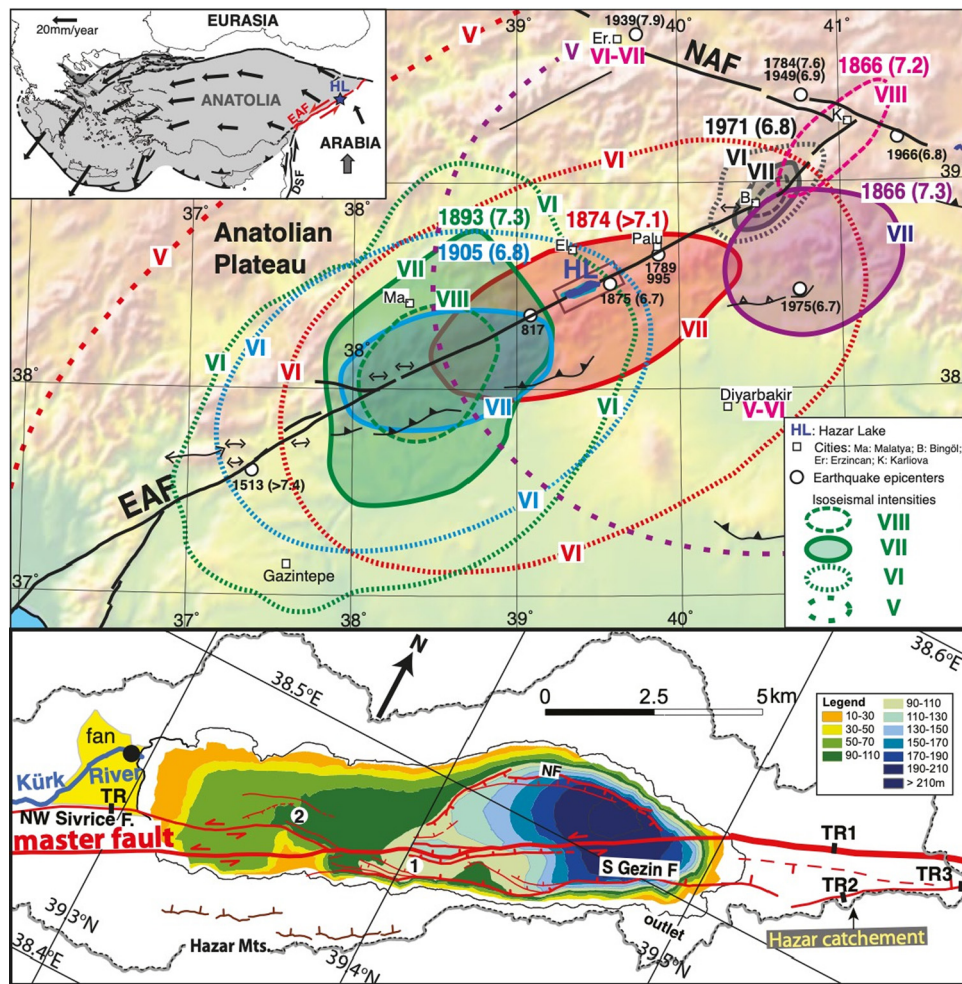
Fig. 1. General setting. **Top inset:** Geodynamics framework of the East Anatolian Fault (EAF in red) that accommodates the Anatolian extrusion away from the Arabian plate. GPS data from Reilinger et al. (2006). H.L (Hazar Lake) and blue star indicate the study location. **Top**: EAF fault map with isoseismal intensity of 19th century earthquakes closely associated with the East Anatolian Fault Zone (EAFZ), in 1893 (M = 7.1), in 1905 (M = 6.8), in 1874 (M = 7.1), in 1866 (2 shocks of M = 7.2 and 7.3). White circles indicate the locations of other historical earthquakes close to EAFZ in 817, 995, 1513, 1875, 1975, and along the North Anatolian Fault (NAF) in 1784, 1939, 1949. **Bottom**: Coring location in Hazar Lake crossed by the EAF (sites 1 and 2). Kürk Delta is indicated with location of paleo-liquefaction features with a black circle (Hubert-Ferrari et al., 2017). Paleoseismic trenches (TR 1, 2, 3, Table 2) of Çetin et al. (2003) and of Garcia-Moreno et al. (2011) (TR) are indicated. (For interpretation of the colors in the figure(s), the reader is referred to the web version of this article.)

the historical seismicity and paleoruptures identified in trenches to confirm a seismic trigger. Finally using this new paleoseismic data we discuss the seismic versus aseismic motion of the East Anatolian Fault.

2. Seismotectonic and sedimentological setting

The EAF is a major left-lateral strike-slip fault in Turkey that extends over 600 km from its junction with the NAF in the East Anatolian Plateau (Hubert-Ferrari et al., 2009) to its junction with the Dead Sea Fault near the Mediterranean Sea (Yönlü et al., 2017; Fig. 1). The EAF is highly segmented with short individual segments (Duman and Emre, 2013). Its segmentation suggests a maximum magnitude threshold lower than along the NAF. In addition, background seismic activity is located on secondary sub-parallel faults whereas the main strand shows little activity (Bulut et al., 2012) and creep (Cavalié and Jonsson, 2014).

The EAF accommodates most of the plate motion between Anatolia and Arabia with minor intraplate deformation (Reilinger et al., 2006). Its slip ranges from 13 to 9 mm/yr (Reilinger et al., 2006; Cavalié and Jonsson, 2014), but InSAR data suggest the occurrence of creep (Cavalié and Jonsson, 2014). The inferred shallow locking depth of ∼4.5 km implies either a nearly full creep of the fault

or a narrow compliant zone around the fault that accommodates most of the near-surface deformation.

The Hazar Basin is a tectonic extensional basin located in the central part of the EAF (Fig. 1). Lake Hazar occupies a large part of this basin that is crossed by a single NE-trending master fault (Garcia-Moreno et al., 2011). Several secondary faults are present. In the eastern half of the lake, two sets of normal faults bound a deep lacustrine sub-basin to the north and south. The southern normal fault system extends onland to the northeast of Lake Hazar and was called the Gezin Fault by Çetin et al. (2003), the activity of which is confirmed in paleoseismic trenches (Fig. 1; Table 2). In the western half of the lake, the Sivrice Fault runs subparallel to the master fault across a relatively flat ∼90 m deep lacustrine sub-basin, and extends onland bounding to the south of an alluvial fan built by the largest inflowing Kürk River.

The area around Lake Hazar has been struck by several large earthquakes (Fig. 1; Table 1). The most recent significant earthquake occurred during the 19th century on 3 May 1874 (Ambraseys, 1989). The M∼7.1 earthquake was preceded by foreshocks of large magnitude. This earthquake rupture was evidenced in paleoseismic trenches NE of Lake Hazar as a ∼40 cm offset on the Gezin Fault (Çetin et al., 2003; Fig. 1; Table 2), and on seismic reflection profiles in the SW part of the lake

Table 1
Historical earthquakes and paleoearthquakes around the East Anatolian Fault.

Date	Location and/or main city close to Epicenter	Magnitude and/or destructions	Distance from Hazar L.	Reference
AD 1975/09/06	N38.5-E40.7; Lice	6.7; Io = X	~110 km	1, 2, 3
AD 1971/05/22	N38.9-E40.5; Bingol	6.8 Io = X	~115 km	1, 2, 3
AD 1966/08/19	N39.2-E41.5; Varto	6.8	~190 km	2, 3
AD 1949/08/17	N39.6-E40.5; Emali	6.9	~140 km	2, 4, 3
AD 1905/12/04	N38.1-E38.6; Pütürge and Celikan	6.7-Io = IX; Destruction with great loss of life.	~75 km	1, 3, 5
AD 1897/07/03	Malatya		~85 km	6
AD 1897/09/09	Palu		<50 km	6
AD 1896	Malatya	Strong shock felt	~85 km	6
AD 1893/03/02	N 38.0-E38.3; Malatya	>7.1; Io = X	~85 km	3, 6
AD 1890/11/07	Malatya	Strong earthquake felt	~85 km	6
AD 1884/02/10	Siirt	6.9; Io = VIII		1, 6
AD 1875/03/27	N38.5-E39.5; Sivrice; Palu	6.7; Io = VII; Hazar water-level change	0 km	1, 3
AD 1874/05/03	N38.5-E39.5; Sivrice; Palu	>7.1; Io = XI water-level change, large radius of destruction	0 km	1, 3
AD 1872/04/03	N36.4-36.4; Antakya	<7.2; Io = X	~350 km	1, 3
AD 1871/03/17		>6.8		1
AD 1866/05/12	N39.2-E41.0; Gönek	7.2; 45 km fault rupture	~130 km	3, 4
AD 1866/06/20	Kulp-	Ms < 6, 8;	~130 km	1
AD 1855/01/16	Tarsus	Strong shocks	~200 km	6
AD 1789/05/28	Palu, district Tunceli, area Keban dam	>7; Io = X; destructions radius 75 km; 51000 death	<50 km	1, 7
AD 1779/03/14	Malatya, Divrigi	Destruction mostly in Divrigi and Malatya, death Ovacik Valley	~100 km	6, 7
AD 1784/07/18	Emali		~125 km	3, 8
AD 1583/06/27	Emali		~125 km	8
AD 1544	Zitun, Maras and north	6.7	~200 km	6
AD 1514-1513	Adana, Tarsus, Malatya EAF SW Gölalanı	>7.4->340 km radius of destruction	~200 km	1, 6, 11
AD 1284-1285 (winter)	Malatya, Bar Suma	Damaging earthquake	~85 ± 10 km	9
AD1285	Malatya	Damaging earthquake: Collapse Monastery Bar Suma	~85 km	6
AD 1275/10/03	Malatya		~85 km	9
AD 1157/08/12	Malatya		~85 km	6
AD 1149/12/29	Malatya		~85 km	9
AD 1145/05/24	Malatya		~85 km	9
AD 1140/10/29	Malatya		~85 km	9
AD 1127 Fev-Nov	Malatya	Several	~85 km	9, 10
AD 1121/12/18	40 km NW Malatya, Euphrates R.	8 shocks, cracks, and inhabitant shallowed	~40 km	9
AD 1120/01/01	Malatya	violent earthquaje destroyed many places	~85 km	9, 10
AD 1114/11/29	Maras, EAF NE Gölalanı	>7	~200 km	6, 1, 11
AD 1108	Malatya	Strong with collapse in many places	~85 km	9
AD 1103/02	Malatya		~85 km	9
AD 1003	Al-Thughur, Malatya	Large destruction and causualty		6
AD 995/08/19	Palu, Sivrice	Total destruction cities associated with deformation, water level changes	0 km	3, 6
AD 817 Aug Claudias	Euphrates R. bend in Claudi Region between Malatya and Elazig	large landslide	~40 km	6
AD 601/04/2	Surb Karapet	Destructions northern Syria-southern Anatolia		6
AD 300 May 14	Tarsus		~200 km	6

1: Ambraseys, N.N. (1989). Temporary seismic quiescence: SE Turkey. Geophysical Journal International, 96(2), 311-331; 2: Nalbant, S.S., McCloskey, J., Steacy, S., & Barka, A.A. (2002). Stress accumulation and increased seismic risk in eastern Turkey. Earth and Planetary Science Letters, 195(3-4), 291-298; 3: Ambraseys, N.N., & Jackson, J.A. (1998). Faulting associated with historical and recent earthquakes in the Eastern Mediterranean region. Geophysical Journal International, 133(2), 390-406; 4: Ambraseys, N.N. (1997). The little-known earthquakes of 1866 and 1916 in Anatolia (Turkey). Journal of Seismology, 1(3), 289-299; 5: Ambraseys, N.N., & Finkel, C.F. (1987). Seismicity of Turkey and neighbouring regions, 1899-1915. In Annales geophysicae. Series B. Terrestrial and planetary physics (Vol. 5, No. 6, pp. 701-725); 6: Ambraseys, N. (2009). Earthquakes in the Mediterranean and Middle East: a multidisciplinary study of seismicity up to 1900. Cambridge University Press; 7: Ambraseys, N.N.N., & Finkel, C.F. (1995). Seismicity of Turkey and Adjacent Areas: A Historical Review, 1500-1800. MS Eren; 8: Zabcı, C., Akyüz, H.S., & Sançar, T. (2017). Palaeoseismic history of the eastern part of the North Anatolian Fault (Erzincan, Turkey): Implications for the seismicity of the Yedisu seismic gap. Journal of Seismology, 21(6), 1407-1425; 9: Guidoboni, E., Comastri, A., & Storia, S.G.A. (2005). Catalogue of Earthquakes and Tsunamis in the Mediterranean Area from the 11th to the 15th Century; 10: Ambraseys, N.N. (2004). The 12th century seismic paroxysmin the Middle East: a historical perspective. Annals of Geophysics; 11: Karabacak, V., Yönlü Ö, Altunel, E., Kıyak, N., Akyüz, S., Yalçıner, C. (2012). Paleoseismic behavior of the East Anatolian Fault Zone between Gölbaşı and Türkoğlu: implications on 900 yrs of seismic quiescence. International Earth Science Colloquium on the Aegean Region, IESCA-2012 1-5 October 2012, Izmir, Turkey.

Table 2
Paleoseismic trenches results from Çetin et al. (2003) across the normal Gezin Fault (TR2 and TR3) and across the main EAF strand (TR1).

Trenches	Events	Evidences	^{14}C samples	Bulk age	Calibrated ages
TR2	Event 1	40 cm offset at a stream deposit unit	Stream deposit	70 ± 40	AD 1682-1939
	Event 2	Scarp derived colluvium 3	Base of colluvium 3	490 ± 40	AD 1393-1464
	Event 3	Scarp derived colluvium 2	Bones inside colluvium 2	1550 ± 40	AD 418-594
			Charcoal layer at base colluvium 2	1580 ± 70	AD 333-630
	Event 4	Scarp derived colluvium 1	–	–	
TR3	Event 1	Fissures filled with organic soil	Base of organic soil filling fissures	1820 ± 40[*]	AD 235-406
TR1	Possible Ev1	Debris facies colluvium			
	Possible Ev 2	Colluvial wedge 2b	Base colluvial wedge 2b	2670 ± 40	BC 901-796
	Event 3	Colluvial wedge 2a and fault termination at its base and extremity	–	–	
	Event 4	Scarp derived colluvial wedge 1 with fault termination	Colluvial wedge 1	4760 ± 90	BC 3706-3360

[*] Organic soil may have a ∼100 yrs old reservoir age according to Çetin et al. (2003).

(Hubert-Ferrari et al., 2017). These findings suggest that the 1874 earthquake ruptured fault segments on both sides of the lake. On 27 March 1875, a second M∼6.7 event occurred. This earthquake rupture was evidenced in a seismic reflection profile at the SW end of the lake along the Sivrice Fault (Hubert-Ferrari et al., 2017). Based on historical data, earthquakes in 1789 and 995 may have also ruptured the EAF, near Palu, NE of the Hazar Lake (Ambraseys, 1989). In addition, in 1866 a M∼6.7 earthquake (associated with a ∼45 km long surface rupture) occurred near Bingöl to the NE of Lake Hazar (Ambraseys, 1989). Two other earthquakes occurred in the south-west of Lake Hazar, i.e. 1893 M∼7.3 earthquake near Malatya and 1905 M∼6.7 earthquake near Pütürge (Fig. 1). The characteristics of the other historical earthquakes and paleoearthquakes inferred to have occurred along the East-Anatolian Fault are summarized in Table 1. The isoseismal intensities of 19th and 20th century earthquakes are included in Fig. 1.

Lake Hazar sediments have been demonstrated as an archive sensitive to earthquake shaking in several instances. First, seismites and other soft sediment deformation structures were documented in and around the lake. For example, the Kürk Delta of Lake Hazar (Fig. 1) displays recurrent soft-sediment deformation structures and liquefaction features attesting to sustained strong earthquake shaking (Hubert-Ferrari et al., 2017). The last two liquefaction episodes were associated with the 1874/1875 sequence and the 1789 earthquake in Hubert-Ferrari et al. (2017). Second, short cores collected from the near shore deltaic environment evidenced two large sedimentary event deposits related to density flows probably induced by earthquake induced landslides triggered by the 1874 and 1875 earthquakes (Hubert-Ferrari et al., 2017). Third, sediment cores from the deeper part of the lake have also been hypothesized as a record of earthquakes in Hage et al. (2017). The latter study documented the occurrence of thin clayey sand turbidites at different locations and their depositional processes. Three types of turbidites are distinguished. Type 1 is made of an ungraded clayey silt layer issued from a cohesive flow. Type 2 is composed of a partially graded clayey sand layer overlain by a mud cap, attributed to a transitional flow. Type 3 corresponds to a graded clayey sand layer overlain by a mud cap issued from a turbulence-dominated flow. The different type of turbidites reflect different initial amount of reworked sediments and the dilution of the flow along its path. Turbidites are proposed to result from superficial slope remobilization of the lacustrine sediments, most likely triggered by earthquake shaking. A seismic trigger was inferred given the turbidite characteristics and the fact that different sources were activated during their emplacement, which implies a regional trigger. In the present study, we focus on the sites used in Hage et al. (2017) to infer the depositional history of these turbidites.

Lake Hazar sediments is also an archive sensitive to climate changes (Eriş, 2013; Eriş et al., 2018). It is an oligotrophic, hardwater, alkaline soda lake (pH around 9.3, salinity 16%) that is close most of the time. It spills to the Tigris River through a faulted outlet only during its highest stand, and during the late Holocene period has sustained large >30 m water level changes most probably related to climatic changes (Hubert-Ferrari et al., 2017; Eriş, 2013).

3. Materials and methods

We worked on two sites that independently record the occurrence of past turbidity currents (Hage et al., 2017; Fig. 1). Site 1, at 99 m water depth, is located near the faulted southern margin. Site 1 stands a few hundred meters away from the turbidity current sources. These sources are inferred to consist of a thin veneer of sediments covering the steep faulted slopes along the lake margin. Site 1 cannot be reached by hyperpycnal flows related to extreme rainfall events because it is located far from the main streams. Site 2 is at 72 m water depth and is located in the middle of a flat sub-basin in the southwestern half of the lake. The subaqueous sources of turbidity currents reaching site 2 are the gentle slopes of sublacustrine delta fronts lying at 50 m water depth along the lake shore (Eriş, 2013). The largest source is the Kürk Delta front located at the lake's western end, ∼3 km west of site 2. Site 2 might be impacted by hyperpycnal flows related to extreme rainfall events striking the Kürk River catchment (Eriş et al., 2018) and by human related environmental changes on the subaerial part of the delta.

Cores at site 1 comprise two up to ∼1.1 m long gravity cores and a 4.5 m long piston core. Cores at site 2 include two gravity cores and two 3.5 and 4.9 m long piston cores (Figs. 2, 3). The top of the 4.9 m long core at site 2 is missing, so a composite core combining the two long cores was built.

High resolution X-Ray radiograms were acquired on the short and long cores. XRF geochemical measurements were performed every 2 mm with an AVAATECH core scanner. Physical properties were measured every 5 mm using a GEOTEK multi-sensor core logger (MSCL). Magnetic susceptibility, density, Fe/Ca ratio and Ca/Ti ratio were used in the present study. In addition, loss of ignition analyses were performed at 1 cm resolution to infer organic matter and carbonate contents. Correlation between carbonate, organic content and Ca/Ti ratio observed in the short cores at both sites implies that Ca/Ti ratio can be used as a proxy for carbonate content and productivity (Hage et al., 2017; Fig. 2). Correlation between magnetic susceptibility, density and Fe/Ca ratio implies that the latter is a good proxy for terrestrial supply. Geochemical and geophysical properties of the sediments were used to identify turbidites, turbidite types following Hage et al. (2017) and to infer lake level changes.
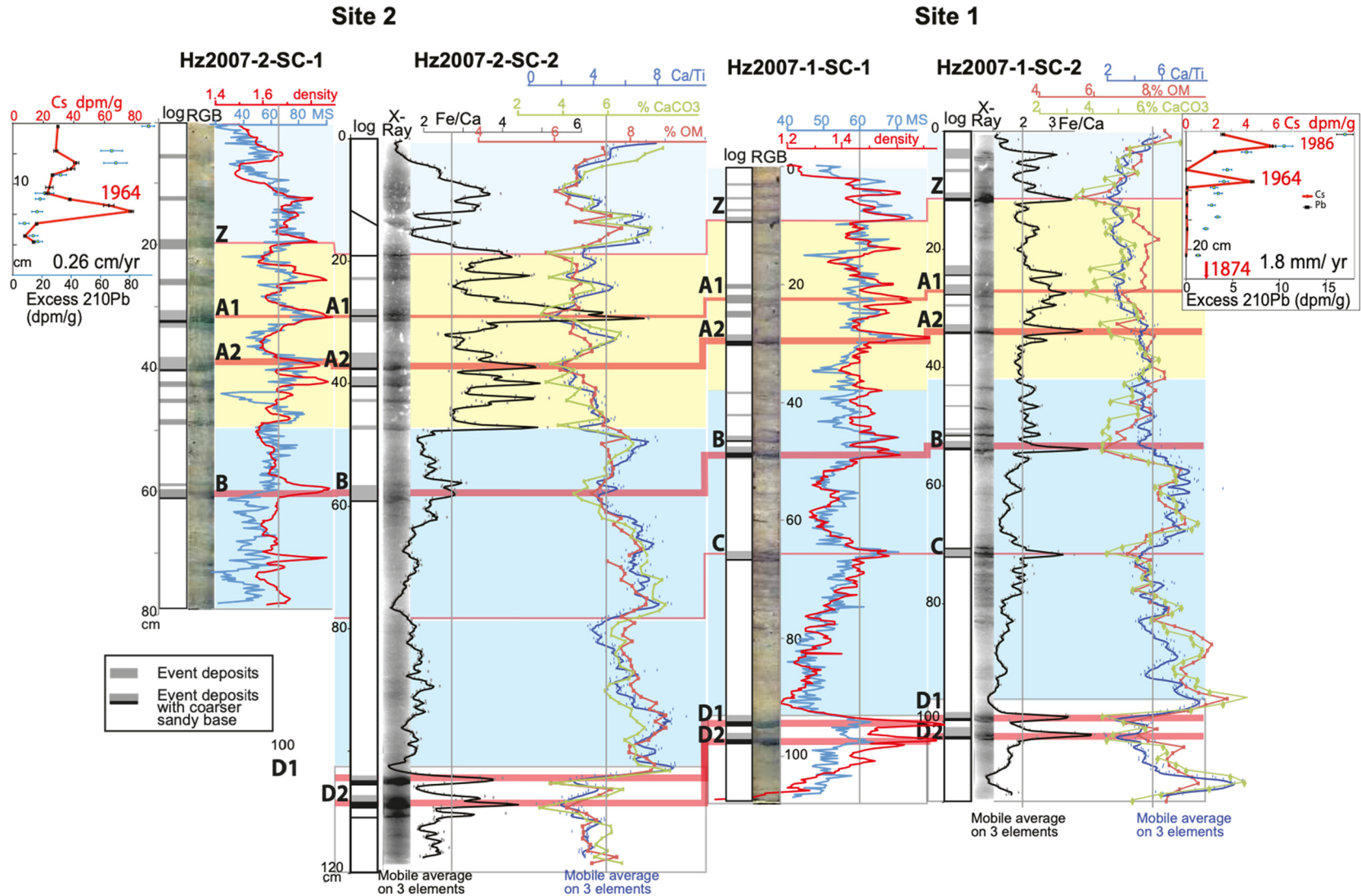
Fig. 2. Multi proxi-analyses on short cores and inferred correlation between sites 1 and 2. **Right:** site 1 cores with (1) core HZ2007-1-SC-1, log with identified event deposits, Cs/Pb measurements and RGB image, MS and density, and with (2) core HZ2007-1-SC-2, log with identified event deposits, X-Ray Scopix images, Fe/Ca ratio, organic matter and carbonate contents correlating with Ca/Ti ratio. **Left:** site 2 cores with (1) core HZ2007-2-SC-1, log with identified event deposits, RGB image, MS and density obtained on a GEOTEK Scanner, and with (2) core HZ2007-2-SC-2, log with identified event deposits, X-Ray Scopix images, Fe/Ca ratio, organic matter and carbonate contents correlating with Ca/Ti ratio and Cs/Pb measurements. Correlation is indicated with in blue, low stands (high carbonate and organic content due to an increase in primary productivity, low terrigenous input) and in yellow, high stands (high terrigenous input due to increase erosion by rainfall, low carbonate due to dilution). The top yellow strip corresponds to the 19th century highstand (Hubert-Ferrari et al., 2017; Hage et al., 2017). Cs and Pb dating provide a sedimentation rate indicated and imply that event Z is a human induced disturbance.

Fig. 3. Multi proxi-analyses in long cores and correlation between sites 1 and 2 with yellow bands indicating lowstands and blue bands highstands. Classification of turbidites following Hage et al. (2017). Event labeling size is done according to the amount of sediment remobilized. **Right:** site 1 long core with the HZ2007-1-LG-4.6m core, log with identified event deposits, X-Ray Scopix images, RGB image, location of radiocarbon samples (light blue: macroplants; dark blue: bulk samples), Magnetic Susceptibility (MS), Fe/Ca and Ca/Ti ratio. **Left:** site 2 long cores with (1) HZ2007-2-LG-4.9m core, log with identified event deposits, RGB image, location of radiocarbon samples (light blue: macroplants; dark blue: bulk samples), MS and with (2) HZ2007-2-LG-3.5m, log with identified event deposits, X-Ray Scopix images, Fe/Ca and Ca/Ti ratio. **Far left:** composite log with correlative events studied here.

Table 3

Correlative sedimentary event deposits with depth as in core Hz2007-2-LG-4.9m and radiocarbon dating samples with depth location in original cores and in the composite core (corrected from event deposit thickness); in grey samples from site 2; in bold, plant remains. All radiocarbon dating done on bulk sediments are a table as Supplemental Material.

Name	Type	Original depth[a] (mm)	Depth[b] (mm)	Age yr BP	Age Error
Hz2007-2-LG-4.9m	Bulk sediment*	4988	5081	4820	35
Event P	*Sedimentary event*	*4760*	*4853*		
Event O	*Sedimentary event*	*4560*	*4653*		
Hz2007-2-LG-4.9m	Sediment*	4213	4306	4390	40
Event N	*Sedimentary event*	*4210*	*4303*		
Hz2007-2-LG-4.9m	**Macro plants**	**4190**	**4298**	**2860**	**30**
Event M	*Sedimentary event*	*4090*	*4198*		
Hz2007-2-LG-4.9m	Bulk sediment*	3988	4126	4230	30
Hz2007-2-LG-4.9m	Bulk sediment*	3723	3866	3570	35
Event L	*Sedimentary event*	*3720*	*3858*		
Event K	*Sedimentary event*	*3470*	*3638*		
Hz2007-1-LG-4.5m	Bulk sediment*	4655	3605	3460	30
Hz2007-2-LG-4.9m	**Macro plants**	**3325**	**3503**	**2000**	**25**
Hz2007-1-LG-4.5m	Bulk sediment*	4508	3499	3270	30
Hz2007-1-LG-4.5m	Bulk sediment*	4363	3388	3150	25
Event J	*Sedimentary event*	*3200*	*3378*		
Hz2007-1-LG-4.5m	**Macro plants**	**4240**	**3305**	**1760**	**30**
Hz2007-1-LG-4.5m	**Macro plants**	**4130**	**3232**	**1595**	**30**
Event I	*Sedimentary event*	*3050*	*3228*		
Hz2007-2-LG-4.9m	**Macro plants**	**2915**	**3103**	**1635**	**20**
Hz2007-1-LG-4.5m	**Macro plants**	**3995**	**3078**	**1600**	**25**
Hz2007-1-LG-4.5m	Bulk sediment*	3923	3025	2800	30
Event H	*Sedimentary event*	*2822*	*3012*		
Hz2007-1-LG-4.5m	**Macro plants**	**3860**	**2993**	**1560**	**30**
Event G	*Sedimentary event*	*2822*	*2790*		
Hz2007-1-LG-4.5m	Bulk sediment*	3413	2727	2710	30
Hz2007-2-LG-4.9m	**Macro plants**	**2255**	**2464**	**1420**	**30**
Event F2	*Sedimentary event*	*2210*	*2388*		
Hz2007-1-LG-4.5m	**Macro plants**	**2820**	**2356**	**1340**	**35**
Hz2007-1-LG-4.5m	Bulk sediment*	2803	2342	2090	30
Event F1	*Sedimentary event*	*2210*	*2248*		
Hz2007-1-LG-4.5m	Bulk sediment*	2593	2114	1950	30
Hz2007-2-LG-4.9m	**Macro plants**	**2255**	**2011**	**1160**	**20**
Event E2	*Sedimentary event*	*2238*	*1996*		
Event E1	*Sedimentary event*	*2210*	*1952*		
Hz2007-1-LG-4.5m	**Macro plants**	**2400**	**1935**	**985**	**25**
Event D2	*Sedimentary event*	*1478*	*1670*		
Event D1	*Sedimentary event*	*1478*	*1614*		
Hz2007-1-LG-4.5m	**Macro plants**	**1570**	**1367**	**235**	**30**
Hz2007-1-LG-4.5m	**Macro plants**	**1530**	**1342**	**475**	**30**
Event C	*Sedimentary event*	*840*	*1247*		
Hz2007-2-LG-4.9m	**Macro plants**	**825**	**1237**	**260**	**25**
Hz2007-1-LG-4.5m	**Macro plants**	**1170**	**973**	**340**	**30**
Hz2007-1-LG-4.5m	**Macro plants**	**1095**	**864**	**230**	**30**
Event B	*Sedimentary event*	*825*	*841*		
Event A2	*Sedimentary event*	*270*	*432*		
Event A1	*Sedimentary event*	*145*	*285*		
Event Z	*Sedimentary event*		*149*		

[a] Sedimentary Event depth taken in Hz2007-2-LG-4.9m.
[b] Depth in Composite core corrected from event deposit thickness and top core (mm).
* Bulk sample used in the age model.

Table 4

68% and 95% confidence age intervals of sedimentary events with two Oxcal P sequence model, the first one including only macroplant samples and the second one including some selected bulk samples (as indicated in Fig. 3 and in Table 3).

Name	Depth* (mm)	Modeled ages including only macroplants		Modeled ages with some bulk samples	
		68.2% probability	95.4% probability	68.2% probability	95.4% probability
Event P	4853	(0.2%) 1380-1378 BC (0.2%) 1376-1374 BC (67.3%) 1372-1018 BC (0.5%) 1017-1013 BC	(95.4%) 1812-952 BC	(68.2%) 1478-1360 BC	(95.4%) 1544-1308 BC
Event O	4653	(0.5%) 1269-125 BC (67.7%) 1264-1015 BC	(0.2%) 1546-1541 BC (95.2%) 1540-951 BC	(68.2%) 1328-1228 BC	(95.4%) 1383-1182 BC
Event N	4303	(7.0%) 1110-1098 BC (15.4%) 1091-1062 BC (45.7%) 1057-997 BC	(95.4%) 1124-930 BC	(68.2%) 1061-990 BC	(92.9%) 1111-970 BC (2.5%) 962-948 BC
Event M	4198	(68.2%)1061-936.5 BC	(95.4%) 1113-862 BC	(68.2%) 995-910 BC	(95.4%) 1043-874 BC
Event L	3858	(68.2%)650-482 BC	(95.4%) 727-394 BC	(68.2%) 553-438 BC	(0.3%) 692-688 BC (0.4%) 687-682 BC (94.7%) 662-397 BC
Event K	3638	(68.2%)261-137 BC	(95.4%) 329-84 BC	(68.2%) 291-183 BC	(95.4%) 336-127BC
Event J	3378	(2.0%) 310-313 AD (1.2%) 315-317 AD (65.0%) 347-384 AD		(46.5%) 281-327 AD (21.7%) 351-373 AD	(95.4%) 257-382 AD
Event I	3228	(3.8%) 361-364 AD (64.4%: 384-405 AD	(23.7%) 348-375 AD (71.7%) 379-409 AD	(50.0%) 348-369 AD (18.2%) 388-398 AD	(63.0%) 342-377 AD (32.4%) 380-405 AD
Event H		(68.2%) 425-442 AD	(95.4%) 417-453 AD	(68.2%) 423-442 AD	(95.4%) 415-455 AD
Event G	2790	(68.2%) 460- 497 AD	(95.4%) 445-519 AD	(68.2%) 465-507 AD	(95.4%) 452-532 AD
Event F2	2388	(68.2%) 643- 680 AD	(95.4%) 627-706 AD		
Event F1	2248	(68.2%) 738-789 AD	(95.4%) 715-816 AD		
Event E2	1996	(68.2%) 937- 969 AD	(95.4%) 925-989 AD		
Event E1	1952	(68.2%) 991 AD-1023 MAD	(95.4%) 969-1036 AD		
Event D2	1670	(46.7%) 1199-1247 AD (21.5%) 1292-1325 AD	(95.4%) 1186-1340 AD		
Event D1	1614	(43.0%) 1247-1275 AD (25.2%) 1351-1371 AD	(55.1%) 1230-1283 AD (40.3%) 1326-1378 AD		
Event C	1247	(33.6%) 1516-1533 AD (34.6%) 1636-1653 AD	(48.5%) 1506-1544 AD (46.9%) 1627-1661 AD		
Event B	841	(27.9%) 1661-1676 AD (40.3%) 1797-1811 AD	(48.4%) 1651-1688 AD (47.0%) 1794-1816 AD		
Event A2	432	(28.1%) 1827-1853 AD (40.1%) 1882-1907 AD	(47.4%) 1812-1871 AD (48.0%) 1872-1912 AD		
Event A1	285	(68.2%) 1911-1939 AD	(95.4%) 1891-1944 AD		

* Depth in composite core corrected from event deposit thickness.

Sediment chronology was constrained by radiocarbon dating on terrestrial macroplants and on the bulk organic fraction (Table 3, and Table in Supplemental Material). Radionuclide dating (^{210}Pb and ^{137}Cs) was further used in the upper part of the gravity cores (Fig. 2). We directly use the radiocarbon ages obtained from macroplants to infer the timing of the lake level changes. We build a long composite log combining all radiocarbon ages at site 1 and 2 to obtain a more accurate age model for the turbidites chronology (Fig. 3). In the age-depth model, we removed all identified event deposits, and corrected the depth of the radiocarbon-dated samples accordingly. We used a Bayesian depositional model implemented in the Oxcal software labeled P_sequence that can account for changes in deposition rates (Ramsey, 2008). The sedimentary sequence was broken in several parts using the implemented function Boundary that represents change in sedimentation and possibly sedimentation rates. In Lake Hazar, boundaries were set-up at water-level changes identified in the multi-proxy analyses. Radionuclide dating was used as anchor points at the core top in the Oxcal model. A first P_sequence was run using ages obtained from the macroplants (Table 4). Finally, some bulk ages listed in Table 3 were used to refine the model after an evaluation of the reservoir ages.

4. Results and discussion

4.1. Sedimentation and lake level changes

Sediments in all cores are composed of clayey silt with a few cm-thick intercalated thin clayey sand layers interpreted as turbidites (Hage et al., 2017). The geochemical and geophysical proxies show an alternation of sedimentary units with i) high carbonate content, high organic matter content, high Ca/Ti ratio and low MS and Fe/Ca ratio, ii) units showing the opposite properties. These cyclic changes are similar at the two sites, and are attributed to lake level fluctuations (Eriş, 2013; Hage et al., 2017).

The record in the short cores (Fig. 2) and the corresponding one in the long cores (top 1.7 to 2.2 m) (Fig. 3) show three identical major cycles in sedimentation. Radiocarbon (Table 3; Table in Supplemental Material) and radionuclide dating imply that the cycles correspond to historical water level changes (Fig. 2; Hage et al., 2017). Sediment unit at the top with high carbonates and low terrigenous content was deposited during the human induced water level drop starting in ∼1965 due to water pumping. Below this, sediments with low carbonates and high terrigenous content have recorded the 19th century highstand, during which an Armenian monastery on the southwestern shore was submerged (Hubert-Ferrari et al., 2017). The antecedent period is the Little Ice Age characterized by sediments with low terrigenous input, and high carbonates with some fluctuations. This period corresponds to the 12-18th century lowstand during which the Armenian monastery was in use. In the long cores, we identify a large sedimentological change at 330 cm deep at site 1 and at 250 cm at site 2, characterized by a sharp rise in terrigenous input and a drop in carbonates above the corresponding depths. Radiocarbon dating indicates that it could correspond to the AD 530 climatic change as observed in Nar Lake in Central Anatolian (Jones et al., 2006). This interval is followed downward by sediments with the opposite geochemical

characteristics comprising a particular 20 cm thick laminated sequence at site 2 in the 4.9 m long core (Fig. 3).

The alternating geochemical changes related to lake level changes allow a close correlation of the cores between the two sites (Figs. 2 and 3). The correlation was used to build a reliable composite log at site 2, on which we can report all radiocarbon age data obtained from all cores. So we derive a single age depth model (Fig. 3, Table 3).

4.2. Turbiditic occurrence and chronology

The geochemical and geophysical proxies also show sharp peaks of MS and Fe/Ca corresponding to Ca/Si (carbonates) excursions towards low values (Figs. 2 and 3). These small-scale abrupt geochemical changes occur at the location of dense and coarse layers intercalated in the background sedimentary sequence visible to the naked eye. These layers are thin turbidites, whose sedimentological characteristics have been studied by Hage et al. (2017) in the short cores. The turbidites identified in the long cores have identical characteristics to those in the short cores. The same 3 types of turbidites are present and represent an increasing volume of sediment remobilized (Fig. 3). We infer that they have a similar origin. These turbidites represent superficial remobilized lacustrine slope sediments that have been transported and deposited by turbidity currents. The only suggested triggering of the turbidity currents has been seismic shaking (Hage et al., 2017), yet the lack of dating did not confirm this hypothesis. Here we focus on turbidites deposited synchronously at the two study sites, as synchronous initiation of turbidity currents in two distinct sources is considered as a good indicator for earthquake triggering in Van Daele et al. (2015).

The inter-cores correlation at sites 1 and 2 allows the identification of 16 coeval turbidites (Fig. 3). Near core tops, the first correlative turbidites were labeled Z to keep a consistent labeling with the previous study (Hubert-Ferrari et al., 2017). Below, coeval turbidites were labeled from top, event A, to bottom, event K. Very closely spaced (i.e. 2 to 8 cm spaced) turbidites were labeled with the same capital letter flowed by a number (e.g. A1 and A2). The turbidites at sites 2 are usually more subtle, finer grained and thinner than at site 1. The sediment sources of the turbidites at site 1 are close, so the turbidites are generally not diluted and of type 3 (Fig. 3). Site 2 is more distal with respect to sedimentary sources than site 1, so turbidity currents are inferred to be more dilute (see Hage et al., 2017). The 3 different types of turbidites are present (Fig. 3). All turbidites at site 2 can be correlated with the ones at site 1, except for those located above the recent event deposit B, which would be due to the recent anthropic perturbations in the lake and in its catchment (Hubert-Ferrari et al., 2017). In the lowest part of the longest core at site 2, there are five other prominent events (events L to P) that are absent at site 1. This is because coring ended at 4.5 m deep at site 1 and sedimentation rate is higher at site 1 than at site 2. These last five turbidites in site 2 share similar characteristics to the turbidites at shallower level corresponding to turbidites at site 1. We infer the five large old events only identified at site 2 are in continuity with the rest of the sequence observed at both sites and may thus also result from seismic shaking. Therefore, we included these five older events in the age model as discussed in the following.

Site 1 includes a number of turbidites, which cannot be correlated with site 2 (e.g. between events G and H on Fig. 3). This is because site 1 is located closer to the lake shores compared to site 2, thus these turbidites may initiate from other mechanisms than an intense earthquake shaking. Given the absence of correlation with site 2, we choose not to include the turbidites only observed in site 1 in the age model. Similarly, a large number of sedimentary events occurs at the top of the cores including event Z (Fig. 2);

they could be related to the large 20th century anthropic modifications (e.g. railroad construction in the 1930's, tunnels for water pumping in 1957 and 1967, human induced water level changes after 1970, infill and clay extraction on the Kürk Delta). Several anthropic impacts were already identified in short cores sampling the Kürk Delta (see Hubert-Ferrari et al., 2017). These secondary event deposits will thus not be discussed in the present paper.

The age-depth model of the composite-core for site 2 was built as a P sequence in Oxcal using radiocarbon dating (Table 3) and a chronological anchor near the core top derived from ^{137}Cs and ^{210}Pb data (Fig. 2). We first use radiocarbon ages derived from terrestrial macro plants (Table 3). Radiocarbon ages from bulk sediments were problematic because of the large and variable reservoir pool of old carbon in Lake Hazar (Fig. 4 and Table in Supplemental Material). The offset between the bulk and the macro plant ages ranges from 800 to 1500 yrs, with an average of 1000 yrs. The large changes in reservoir ages are inferred to be related to the water level changes and the variable influx of dead carbon. Yet no straightforward relation between lake level change and variation in reservoir age could be established. Some age variations of the bulk sediments sampled below and above sedimentary events (e.g. events D1 and D2 or event H in Fig. 4) are linked to short-lived changes in the carbon pool. These changes are attributed to the turbidites, which are likely related to strong post-seismic perturbation of the carbon pool. Near the top of the cores the large fluctuations in bulk ages (Fig. 4; Table in Supplemental Material) are inferred to be related to human impacts along the lake shore and in the lake catchment. In particular, the anomalously low reservoir offset of 700-600 yrs near the top at site 2 is attributed to the increase of young carbon from the watershed. We thus used bulk radiocarbon samples to improve the age model only in the interval near the core bottom where they show a more consistent and coherent pattern, and where we have a low density of macroplant samples. The two age models with and without bulk samples are included in Fig. 4 and Table 4.

The model implies that the long record at site 2 spans 3800 yrs. A mean recurrence interval of 190 yrs was obtained for the 20 turbidites A1 to P. This interval is shorter than the inferred ∼350 yrs recurrence interval of earthquakes rupturing the EAF (Çetin et al., 2003; Duman and Emre, 2013). However the present recurrence interval is different form the usual earthquake recurrence interval inferred from paleoseismic trenches. Our recurrence interval represents recurrent earthquake shaking with an intensity equal or larger than V 1/2 at the location of Lake Hazar, because a minimum intensity of V 1/2 was suggested as a threshold to record earthquake shaking in a lacustrine environment by Van Daele et al. (2015). The turbidite record obtained here would thus represent earthquake shaking induced by any source capable of reaching this threshold. For example, earthquakes of magnitude ∼7 on the eastern end of the NAF (i.e. Elmalı segment) or of magnitude ∼8 such as the 1668 NAF historical earthquake would be felt with an MSK intensity VII at the location of the Lake Hazar. Given the central location of Lake Hazar with respect to many different seismic sources (Fig. 1), a recurrence rate of 190 yrs is relatively low.

4.3. Comparison between turbidite record and paleo-historical earthquakes

The ages of the turbidites were compared with those of the historical and paleo-earthquakes. The first set of type 3 turbidites A1 and A2 occurred during the 19th century highstand (Table 4), a conclusion that can be reached independently based on the radionuclide data (Fig. 2). During that highstand, a large liquefaction and lateral spreading episode was documented on the Kürk Delta (Hubert-Ferrari et al., 2017). Additionally, a paleorupture was evidenced in the paleoseismic trench across the Gezin Fault, i.e. the
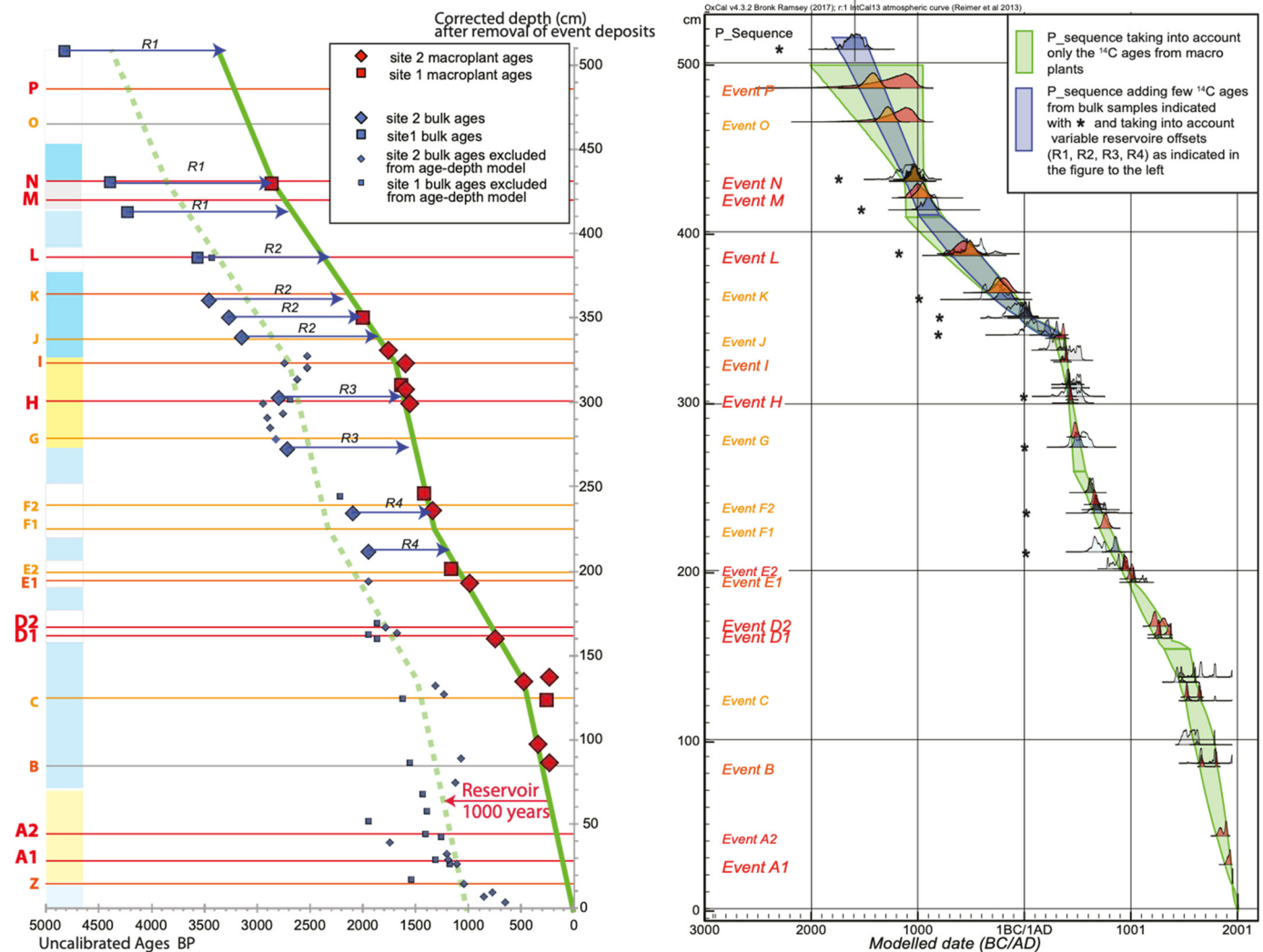
Fig. 4. Age model. **Left**: Bulk and macroplant ^{14}C radiocarbon ages versus their depth in the composite core as in Fig. 3 (see Table in Supplemental Material). We evidence a mean reservoir age of ~1000 yrs with significant variation (R1~1500 yrs; R2~1220 yrs; R3~1200 yrs; R4~750 yrs). Macroplant samples as well as some selected bulk samples listed in Table 3 with the associated reservoir age were used in the age model to the left. **Right**: Oxcal P sequence models representing the modeling event ages in PDF versus depth of the composite log; computed events PDF in orange, PDF of macroplants in grey, PDF of selected bulk samples in blue with an asterisk on the side (associated reservoir offset R1 to R4 as on the left), in green the 95% confidence interval obtained using only macroplant samples and in blue the 95% confidence interval obtained including bulk samples. See also Table 3 for the results.

normal fault system associated with the main strand of the EAF east of Lake Hazar. During that period, two large historical earthquakes struck the study area (1874, 1875), while a burst of seismicity affected a large area centered on the main EAF fault strand (1893 M = 7.1, 1905 M = 6.8 earthquakes southwest of Hazar Lake; 1866 M = 6.8 earthquake at the northeast extremity of the EAF; Ambraseys, 1989). According to the age model, event deposit A2 was most likely triggered by the M = 7.1 1874 and M = 6.7 1875 earthquake sequence and event deposit A1 by the 1893 or 1905 earthquakes, which are associated with an MSK intensity of VI-VII at the location of Lake Hazar. It is coherent with the fact that event deposit A1 is coarser and thicker at site 2, which is influenced by the Kürk Delta, compared to site 1. The 1893-1905 earthquakes would have ruptured faults SW of Lake Hazar, running across the catchment of the Kürk River.

The second event deposit B occurred during AD 1651-1688 (48.4%) or AD 1794-1816 (47%). Radionuclide data imply an occurrence during the second interval (Fig. 4). This event correlates with the earthquake-induced liquefaction features documented on the Kürk Delta that also took place near the lowstand to highstand transition (Hubert-Ferrari et al., 2017). At that time a large M ~

7 earthquake, in 1789, struck the Palu area, which is located just north-east of the Lake Hazar. The event deposit is much coarser at site 1 (Type 3 turbidite) located close to the inferred earthquake source than at site 2 (Type 2 turbidite).

The next two sets of turbidites comprise event deposits C and D1-D2 that occurred during the lowstand period when the submerged Sivrice Armenian settlement was occupied. Two liquefaction events in sediments of the Kürk Delta occurred during that period (Hubert-Ferrari et al., 2017). Event deposit C (Type 1 turbidite) occurred during AD 1506-1544 (48.5%) or AD 1627-1661 (46.9%) (Fig. 4). An extrapolation of the radionuclide-based sedimentation rate favors the second interval. During that period, no large historical earthquake was documented on the EAF. The only paleorupture documented in trenches on EAF east of Lake Hazar is the Tarsus 1513 event, southwest of Gölbaşı Lake (Karabacak et al., 2012; Fig. 1; Table 2) that had a very large radius of destruction (Ambraseys, 1989). In addition, earthquakes occurred in AD 1544 (Zitun earthquake near Maraş, Ambraseys (2009)) near the southwestern end of the EAF, and along the NAF in AD 1583 (Elmali NAF segment, east of Erzincan) and in 1668 (Eastern NAF segment, west of Erzincan) (Ambraseys, 2009). The 1668 earthquake that ruptured

the central and eastern NAF was the largest ever recorded earthquake in Turkey with an inferred magnitude of about 8. If one takes into account a rupture until the city of Erzincan located only 150 km away from Lake Hazar, its inferred magnitude, and the seismic attenuation laws, a seismic intensity larger than VI would be felt at the Lake Hazar location. The 1668 earthquake might thus have emplaced turbidite C that has a very faint expression at site 2. D1 occurred during AD 1326-1378 (40.3%) or AD 1230-1283 (55.1%), and D2 occurred during AD 1186-1340. D1 and D2 are two of the largest sedimentary events with noticeable coarse sandy bases at both sites 1 and 2 (type 3 turbidite). Very little information is available on the historical seismicity during the occurrence period of D1 and D2. However, during the 13th century, destructive earthquakes near Malatya located 85 km west of Lake Hazar (Fig. 1) were reported in AD 1275 (Guidoboni and Comastri, 2005) and AD 1285 (collapse of the monastery of Bar Suma according to Guidoboni and Comastri (2005) and Ambraseys (2009)). During the period, the paleoseismic trench across the normal Gezin fault north-east of Lake Hazar recorded a post-seismic colluvium linked to the reworking of a co-seismic scarp. The base of this colluvium shows a ^{14}C age of 490±40 yrs for the organic sediments (i.e. AD 1324-1393) (Table 2).

The next E1 and E2 events occurred during AD 969-1036 and AD 925-989, respectively (Fig. 4). E1 events are type 2 turbidites similar to event B whereas E2 are more diluted type 1 turbidites. E1 is likely correlated to the 995 historical earthquake, which struck Sivrice and settlements further NE (Palu, Bingöl) (Ambraseys, 2009). E1 may also correspond to the last paleo-liquefaction feature on the Kürk Delta that arose when the lake level increased slightly with respect to the antecedent 18-12th century lowstand.

The events F1-F2 occurred during AD 715-816 and AD 627-706, respectively (Fig. 4). At that time, the AD 817 Aug Claudias earthquake struck the bend of the Euphratus River located 25 km SW of the Hazar Lake between Malatya and Elazig, and it caused a large landslide according to Ambraseys (2009). F1 and F2 are more diluted type 2 turbidite at site 1 than the usual type 3 turbidite. At site 2, F1 event is represented by coarser type 2 turbidite than that for F2 event and is likely correlated with the AD 817 historical event.

There are four events that rapidly occur in less than 230 yrs: event G, AD 445-519; Event H, AD 417-453, event I: (23.7%) AD 348-375, (71.7%) AD 379-409; event J: AD 290-389 AD (Fig. 4). Event H includes the coarsest grain-size content at the two sites whilst event G has a coarse grain content only at site 1 (i.e. type 1 turbidite at site 2). Çetin et al. (2003) documented the occurrence of one paleorupture on the Gezin normal fault east of Lake Hazar. This paleorupture was evidenced from the burial of an old skeleton of a 11 yr-old child with a ^{14}C age of 1550 ± 40 yrs (i.e. AD 418-594) and of a fireplace with a ^{14}C age of 1580 ± 70 yrs (AD 333-630). Events H or G correlate with this paleorupture. Finally, event K occurred during interval 291-183 BC and a paleo-earthquake rupturing the EAF in the 200-400 BC interval was document in paleoseismic trench NE of Gölalanı (Karabacak et al., 2012).

Finally, we used the earthquake catalogue of Tan et al. (2008) combined with those of Ambraseys (2009), Guidoboni and Comastri (2005), and Guidoboni et al. (1994) to compute the cumulative number of earthquakes felt around the EAF Zone (Fig. 5). We compare this number with our historical catalogue of seismic shaking in the Lake Hazar area. Fig. 5 evidences seismicity bursts in AD 450, AD 1000-1100 and AD 1250, which correspond to the clustered sedimentary events H and G (AD 420-497), E1 and E2 (AD 937-1023), and D1 and D2 (AD 1199-1371) in the Lake Hazar sediments, respectively.

The agreement between historical or paleo seismicity and turbiditic occurrence confirm that the turbidites were triggered by
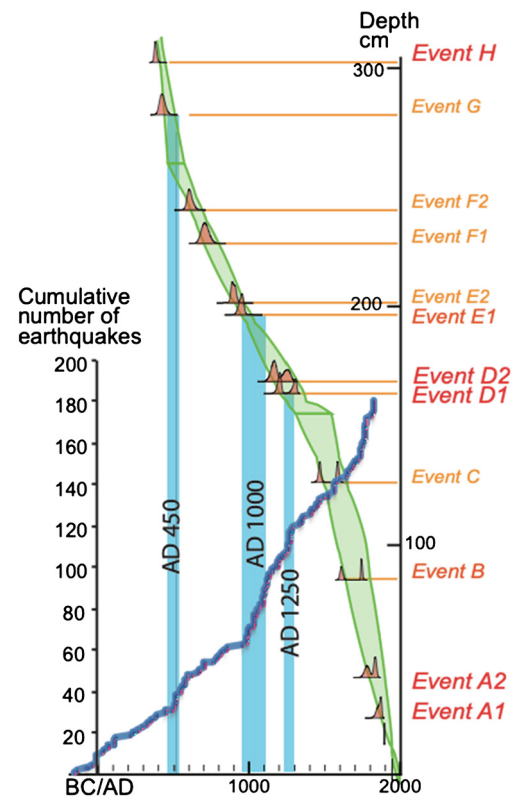

Fig. 5. Comparison with historical seismicity. The PDF event ages versus depth with in green the 95% confidence interval obtained using only macroplant samples in parallel with the cumulative number of earthquakes in the EAF area using the catalogue of Tan et al. (2008) completed with the ones of Ambraseys (2009), Guidoboni and Comastri (2005), and Guidoboni et al. (1994).

slope remobilizations during earthquake shaking. The reason for turbidites occurring in clusters is linked to earthquake clustering. The long-term seismic behavior of the EAF is thus similar to its behavior during 19th to 21st century, i.e. it is characterized by bursts of seismicity that can separated by quiescence periods up to ∼330 yrs long. The Lake Hazar sediment record suggests that bursts of seismicity occurred with variable recurrence interval ranging from 700 to 200 yrs.

4.4. Significance of different type of turbidites

The thin turbidites found in the bottom of Lake Hazar are due to the remobilization of surficial sediments on slopes, and according to Moernaut et al. (2014) the volume remobilized contains information about paleo-earthquake intensity. At site 2, type 1 to type 3 turbidites represent an increasing volume of reworked sediments, and possibly an increasing paleo-intensity. Looking at the distribution of turbidites during the last 3800 yrs, earthquakes with the highest intensity triggering type 3 turbidites would be similar to the M ∼ 7 1874 earthquake that directly stroke the Hazar Lake or to the 1895/1905 earthquakes occurring just SW of the lake. They would have a recurrence of 475 yrs. Large earthquakes rupturing the Palu segment to the NE of the lake like in 1789 or 995 would trigger type 2 turbidites, and would have recurrence of 760 yrs. Other earthquakes triggering type 1 turbidites with a recurrence of ∼540 yrs would represent far field earthquakes.

4.5. Seismic versus aseismic motion of the EAF

The paleoshaking occurrences evidenced in Lake Hazar sediments are in apparent contradiction with creeps documented on

the EAF by the InSAR study of Cavalié and Jónsson (2014). They inferred an interseismic loading rate of 13 mm/yr and full creep up to ∼4.5 km depth. Their inferred shallow locking depth is at odds with the seismogenic depth of 20 km marking the brittle-ductile transition inferred from the seismic studies (Türkelli et al., 2003; Bulut et al., 2012). Preliminary study of Ergintav et al. (2017) using InSAR data, GPS network and creepmeters confirm the occurrence of aseismic creep at the surface, particularly around Lake Hazar. Creep would be variable and could locally reach the interseismic far field plate rate. Creep and the inferred restricted locked depth interval imply a small accumulation of potential energy of elastic deformation and stress increase, and a fault that cannot generate large magnitude earthquakes.

Details about the creep rate, its location, mechanism and origin are still missing. A shallow component of creep could be linked to the occurrence of weak serpentine rocks of the Bitlis suture zone that outcrop near or close to the fault around its central part. A deep creep fraction is also possible given the particular Eastern Anatolian lithosphere that is cut by the EAF. Based on seismic data, this lithosphere is inferred to be composed of a hot 36 to 38 km-thick crust with a missing asthenospheric mantle (i.e. Zor et al., 2003). The latter feature is also confirmed by aeromagnetic, heat flow and gravity data (Bektas et al., 2007). Locally, around Lake Hazar, the magnetotelluric study of Türkoğlu et al. (2015) evidenced a low resistivity zone below the EAF probably related to the occurrence of fluids. The hot fluid-rich lithosphere surrounding the EAF is likely to have a more ductile behavior compared to other continental lithospheres. We thus infer that a deep creep component in the upper crust could be possible around the Lake Hazar area.

Aseismic creep is not systematically incompatible with the occurrence of large magnitude earthquakes. It depends on the size of the creeping zone. Partially creeping faults such as the Hayward fault are still capable of generating Mw ≤ 7 earthquakes at ∼160 yr intervals (Lienkaemper et al., 2012), the last one being the 1868, M = 6.8 earthquake. Furthermore, widespread evidences of creep exist along the NAF in Turkey that ruptured in a series of M ≥ 7 earthquake over 900 km. These large magnitude earthquakes are possible because creep releases only part of the tectonic loading. In the east at the location of the 1939 earthquake, InSAR study by Çakir et al. (2014) point to a shallow 7 ± 2 km locking depth although the seismogenic depth is around 15 km deep. In this eastern location, large paleoruptures were recorded in trenches (Fraser et al., 2012), as well as in paleoshaking-disturbed sediments from shallow lakes (Avşar et al., 2014a). In the central part of the fault, creep occurs for 130 km along the segments that ruptured during the M ≥ 7 1943 and 1944 earthquakes (e.g. Çakir et al., 2005). Full creep is also evidenced locally along these fault segments. Paleoseismic trenches still documented the occurrence of repeated large magnitude earthquakes with surface slip larger than 1 m (Fraser et al., 2010), and paleoshaking was also evidenced in shallow lakes (Avşar et al., 2014b). In the Marmara Sea, creep was inferred in the west along the NAF segment crossing the western high and the Central Basin based on geodetic measurements (Ergintav et al., 2014) and seismicity (Schmittbull et al., 2016). Along a ∼10 km fault patch, the total cumulated slip of the seismic repeaters is similar to geodetic rate implying full creep within the seismogenic zone (Schmittbull et al., 2016). Historical seismicity still evidences that large and clustered earthquakes struck İstanbul and the surrounding shores of the Sea of Marmara (Ambraseys, 2002). Associated paleoshaking was evidenced in sediment cores of the Sea of Marmara. The turbidites infilling the basin were attributed to the rupture of the individual fault crossing the basin and suggest that all NAF segments may rupture in large magnitude earthquakes (McHugh et al., 2006). The sedimentological studies of Drab et al. (2012) and Beck et al. (2015) evidenced a lower number of turbidites in the Central Basin, which is compatible with the occurrence of creep along that particular fault strand.

Coming back to the EAF and the paleoseismic record of seismic shaking recorded in the Lake Hazar sediments, there are still a large uncertainty about the exact size of the creeping patches and their implications regarding seismic hazard assessment. Occurrence of creep along the main EAF segment crossing Lake Hazar is compatible with the lack of frequent paleoseismic ruptures along the main fault in trenches in the east (Çetin et al., 2003): only four potential events were identified in the last 4500 yrs. Similarly, no colluvial wedge was identified west of Lake Hazar across the Sivrice fault scarp (Garcia-Moreno et al., 2011). This is also compatible with the absence of large mass-transport deposits in the lake despite its steep slopes covered with sediments (Hage et al., 2017), and the low volume of remobilized sediments during earthquake shaking (i.e., the largest type 3 turbidites are a few cm thick). If creep occurs along the master fault crossing the Lake Hazar, the surface offsets of the lake floor interpreted to be related to the 1874 and 1875 earthquakes (Hubert-Ferrari et al., 2017) may not be a manifestation of coseismic slip, but could be a delayed surface slip related to the afterslip.

The thin turbidites in Lake Hazar due to the sediment remobilization would start to occur for MSK intensities between V 1/2 and VI according to Van Daele et al. (2015). The earthquake-induced deformational features documented in sections through the Kürk Delta are similar to the ones documented in the Dead Sea triggered by all earthquakes with a local intensity larger than V (Agnon et al., 2006). The gravel liquefaction associated with lateral spreading in the Kürk Delta (Hubert-Ferrari et al., 2017) would require higher paleoshaking intensities. These threshold intensities need to be compared with local recent earthquakes near Lake Hazar. The following earthquakes did not release sufficient energy to impact sediments in and around Lake Hazar: 11/08/2004 Mw = 5.5 Sivrice earthquake with an epicenter at the location of the Kürk Delta, the 21/02/2007 Mw = 5.7 Sivrice earthquake with a normal faulting mechanism located 10 km south of Lake Hazar (Şentürk et al., 2019) and the 8/03/2010 Mw = 6.1 Kovancılar (Elazığ) earthquake, located 60 km NE of Hazar Lake. The larger magnitude M∼7 1874 and M ∼ 6.7 1875 earthquakes, which occurred close to Lake Hazar, are recorded in the Kürk alluvial sediments, in the near-shore lake sediments and in the deep sedimentary infill. The long-term record of turbidites demonstrates that Lake Hazar has repeatedly been subjected to large seismic shaking. Considering the turbidite volume as a possible proxy for paleointensity and the historical seismicity recorded, various seismic sources are inferred. About 65% of all events would be triggered by near field sources linked to the EAF, and the rest would represent the impact of far field sources. The seismic cycle of central EAF is thus only partly impacted by creep.

5. Conclusion

Bottom sediments of Lake Hazar crossed by the EAF were demonstrated to record paleoearthquake occurrence with a 190 yr mean recurrence interval over 3800 yrs. These past earthquakes can be related to a variety of sources: e.g. the main fault segments of the East Anatolian Fault Zone and/or its secondary associated faults, the eastern segments of the North Anatolian Fault. A good correlation between historical earthquake catalogues and measured dates of thin clayey sand turbidites retrieved from Lake Hazar enable a robust reconstruction of the Lake Hazar region paleoseimicity. These turbidites correspond to the 19th century EAF historical sequence (Ambraseys, 1989), the AD 1789 Palu earthquake (Ambraseys, 1989), a 13th century sequence comprising a paleoearthquake evidenced in trenches just east of the Lake Hazar (Çetin et al., 2003), the AD 995 Palu earthquake, the AD 817 Fi-

rat earthquake (Ambraseys, 2009), a 5-6th century EAF paleorupture (Çetin et al., 2003). Our sediment-based earthquake catalogue also evidences that earthquakes occurred in clusters. These earthquake clusters correspond to high frequency of earthquake occurrence documented in the historical seismic catalogue. These seismic bursts would be similar to the 19th century sequence characterized by five earthquakes of magnitude 6.7 to 7 in 1866, 1874-1875, 1893 and 1905. The present study is not in contradiction with the creep documented along the EAF near Lake Hazar, but emphasizes that it remains to be demonstrated how creeping would impact the EAF seismic cycle and the occurrence of large magnitude earthquakes along this plate-boundary. An accurate evaluation of the seismic versus aseismic segments of the East Anatolian Fault Zone, using a combination of InSAR, seismological and paleoseismological studies, is urgently needed in order to improve the seismic hazard assessment of this major intracontinental plate boundary.

Declaration of competing interest

The authors declare that they have no known competing financial interests or personal relationships that could have appeared to influence the work reported in this paper.

Acknowledgements

Appendix A. Supplementary material

Supplementary material related to this article can be found online at https://doi.org/10.1016/j.epsl.2020.116152.

References

Agnon, A., Migowski, C., Marco, S., 2006. Intraclast breccia layers in laminated sequences reviewed: recorders of paleo-earthquakes. In: Enzel, Y., Agnon, A., Stein, M. (Eds.), New Frontiers in Dead Sea Paleoenvironmental Research. In: Geological Society of America Special Paper, vol. 401, pp. 195–214.

Ambraseys, N.N., 1989. Temporary seismic quiescence: SE Turkey. Geophys. J. Int. 96 (2), 311–331.

Ambraseys, N., 2002. The seismic activity of the Marmara Sea region over the last 2000 years. Bull. Seismol. Soc. Am. 92 (1), 1–18.

Ambraseys, N., 2009. Earthquakes in the Mediterranean and Middle East: A Multidisciplinary Study of Seismicity up to 1900. Cambridge University Press.

Avşar, U., Hubert-Ferrari, A., De Batist, M., Lepoint, G., Schmidt, S., Fagel, N., 2014a. Seismically-triggered organic-rich layers in recent sediments from Göllüköy Lake (North Anatolian Fault, Turkey). Quat. Sci. Rev. 103, 67–80.

Avşar, U., Hubert-Ferrari, A., Batist, M.D., Fagel, N., 2014b. A 3400 year lacustrine paleoseismic record from the North Anatolian Fault, Turkey: implications for bimodal recurrence behavior. Geophys. Res. Lett. 41 (2), 377–384.

Beck, C., Campos, C., Eriş, K.K., Çağatay, N., Mercier de Lepinay, B., Jouanne, F., 2015. Estimation of successive coseismic vertical offsets using coeval sedimentary events–application to the southwestern limit of the Sea of Marmara's Central Basin (North Anatolian Fault). Nat. Hazards Earth Syst. Sci. 15 (2), 247–259.

Beckers, A., Beck, C., Hubert-Ferrari, A., Reyss, J.L., Mortier, C., Albini, P., Rovida, A., Develle, A.-L., Tripsanas, E., Sakellariou, D., Scotti, O., Crouzet, C., 2017. Sedimentary impacts of recent moderate earthquakes from the shelves to the basin floor in the western Gulf of Corinth. Mar. Geol. 384, 81–102.

Bektaş, Ö., Ravat, D., Büyüksaraç, A., Bilim, F., Ateş, A., 2007. Regional geothermal characterisation of East Anatolia from aeromagnetic, heat flow and gravity data. Pure Appl. Geophys. 164 (5), 975–998.

Bulut, F., Bohnhoff, M., Eken, T., Janssen, C., Kılıç, T., Dresen, G., 2012. The East Anatolian Fault Zone: seismotectonic setting and spatiotemporal characteristics of seismicity based on precise earthquake locations. J. Geophys. Res., Solid Earth 117 (B7).

Çağatay, M.N., Erel, L., Bellucci, L.G., Polonia, A., Gasperini, L., Eriş, E., Sancar, Ü., Biltekin, D., Uçarkuş, G., Ülgen, U.B., Damcı, E., 2012. Sedimentary earthquake records in the İzmit Gulf, Sea of Marmara, Turkey. Sediment. Geol. 282, 347–359.

Çakir, Z., Akoğlu, A.M., Belabbes, S., Ergintav, S., Meghraoui, M., 2005. Creeping along the Ismetpasa section of the North Anatolian fault (Western Turkey): rate and extent from InSAR. Earth Planet. Sci. Lett. 238 (1–2), 225–234.

Çakir, Z., Ergintav, S., Akoğlu, A.M., Çakmak, R., Tatar, O., Meghraoui, M., 2014. InSAR velocity field across the North Anatolian Fault (eastern Turkey): implications for the loading and release of interseismic strain accumulation. J. Geophys. Res., Solid Earth 119 (10), 7934–7943.

Cavalié, O., Jónsson, S., 2014. Block-like plate movements in eastern Anatolia observed by InSAR. Geophys. Res. Lett. 41 (1), 26–31.

Çetin, H., Güneyli, H., Mayer, L., 2003. Paleoseismology of the Palu–Hazar Lake segment of the East Anatolian fault zone, Turkey. Tectonophysics 374 (3–4), 163–197.

Drab, L., Hubert Ferrari, A., Schmidt, S., Martinez, P., 2012. The earthquake sedimentary record in the western part of the Sea of Marmara, Turkey. Nat. Hazards Earth Syst. Sci. 12, 1235–1254. https://doi.org/10.5194/nhess-12-1235-2012.

Drab, L., Hubert-Ferrari, A., Carlut, J., El Ouhabi, M., Schmidt, S., Martinez, P., 2015. Submarine Paleo-earthquake record of the Cinarcik segment of the North Anatolian Fault in the Marmara Sea (Turkey). Bull. Seismol. Soc. Am. 105, 622–645.

Duman, T.Y., Emre, Ö., 2013. The East Anatolian Fault: geometry, segmentation and jog characteristics. Geol. Soc. (Lond.) Spec. Publ. 372 (1), 495–529.

Ergintav, S., Reilinger, R.E., Çakmak, R., Floyd, M., Cakir, Z., Doğan, U., Özener, H., et al., 2014. Istanbul's earthquake hot spots: geodetic constraints on strain accumulation along faults in the Marmara seismic gap. Geophys. Res. Lett. 41 (16), 5783–5788.

Ergintav, S., Çakir, Z., Doğan, U., Çetin, S., Şenturk, S., Karabulut, H., Julaiti, W., et al., 2017. Aseismic slip and surface creep on the Hazar-Palu Section of the East Anatolian Fault, Turkey. In: AGU Fall Meeting Abstracts. T21A-0540.

Eriş, K.K., 2013. Late Pleistocene–Holocene sedimentary records of climate and lakelevel changes in Lake Hazar, eastern Anatolia, Turkey. Quat. Int. 302, 123–134. https://doi.org/10.1016/j.quaint.2012.12.024.

Eriş, K.K., Arslan, T.N., Sabuncu, A., 2018. Influences of climate and tectonic on the Middle to Late Holocene Deltaic Sedimentation in Lake Hazar, Eastern Turkey. Arab. J. Sci. Eng. 43 (7), 3685–3697. https://doi.org/10.1007/s13369-017-3021-1.

Fraser, J., Vanneste, K., Hubert-Ferrari, A., 2010. Recent behavior of the North Anatolian Fault: insights from an integrated paleoseismological data set. J. Geophys. Res., Solid Earth 115, B9.

Fraser, J.G., Hubert-Ferrari, A., Verbeeck, K., Garcia Moreno, D., Avşar, U., Maricq, N., Vanneste, K., et al., 2012. A 3000-year record of surface-rupturing earthquakes at Gunalan: variable fault-rupture lengths along the 1939 Erzincan earthquake-rupture segment of the North Anatolian Fault, Turkey. Ann. Geophys. 55 (5), 895–927.

Garcia Moreno, D., Hubert-Ferrari, A., Moernaut, J., Fraser, J.G., Boes, X., Van Daele, M., Avsar, U., Çağatay, N., De Batist, M., 2011. Structure and recent evolution of the Hazar basin: a strike-slip basin on the East Anatolian fault, eastern Turkey. Basin Res. 23 (2), 191–207.

Guidoboni, E., Comastri, A., 2005. Catalogue of Earthquakes and Tsunamis in the Mediterranean Area from the 11th to the 15th Century. SGA.

Guidoboni, E., Comastri, A., Traina, G., 1994. Catalogue of Ancient Earthquakes in the Mediterranean Area up to the 10th Century (Vol. 1). SGA.

Hage, S., Hubert-Ferrari, A., Lamair, L., Avşar, U., El Ouahabi, M., Van Daele, M., Boulvain, F., Ali Bahri, M., Seret, A., Plenevaux, A., 2017. Flow dynamics at the origin of thin clayey sand lacustrine turbidites: examples from Hazar Lake, Turkey. Sedimentology 64, 7. https://doi.org/10.1111/sed.12380.

Hubert-Ferrari, A., King, G., Van Der Woerd, J., Villa, I., Altunel, E., Armijo, R., 2009. Long-term evolution of the North Anatolian Fault: new constraints from its eastern termination. Geol. Soc. (Lond.) Spec. Publ. 311 (1), 133–154.

Hubert-Ferrari, A., El-Ouahabi, M., Garcia-Moreno, D., Avşar, U., Altınok, S., Schmidt, S., Fagel, N., Çağatay, M.N., 2017. Earthquake imprints on a lacustrine deltaic system: the Kürk Delta along the East Anatolian Fault (Turkey). Sedimentology 64 (5), 1322–1353.

Jones, M.D., Roberts, C.N., Leng, M.J., Türkes, M., 2006. A high-resolution late Holocene lake isotope record from Turkey and links to North Atlantic and monsoon climate. Geology 34 (5), 361–364.

Karabacak, V., Yönlü, Ö., Altunel, E., Kıyak, N., Akyüz, S., Yalçı, ner C., 2012. Paleoseismic behavior of the East Anatolian Fault Zone between Gölbaşı and Türkoğlu:

implications on 900 years of seismic quiescence. In: International Earth Science Colloquium on the Aegean Region, IESCA-2012, 1-5 October 2012, Izmir, Turkey.

Lienkaemper, J.L., McFarland, F.S., Simpson, R.W., Bilham, R., Ponce, D.A., Boatwright, J.J., Caskey, S.J., 2012. Hayward fault: long-term creep rates suggest a large locked patch controls the size and frequency of its large earthquakes. Bull. Seismol. Soc. Am. 102 (1), 2024–2034.

McHugh, C.M., Seeber, L., Cormier, M.H., Dutton, J., Cagatay, N., Polonia, A., Gorur, N., et al., 2006. Submarine earthquake geology along the North Anatolia fault in the Marmara sea, Turkey: a model for transform basin sedimentation. Earth Planet. Sci. Lett. 248 (3–4), 661–684.

Moernaut, J., Daele, M.V., Heirman, K., Fontijn, K., Strasser, M., Pino, M., Urrutia, R., De Batist, M., 2014. Lacustrine turbidites as a tool for quantitative earthquake reconstruction: new evidence for a variable rupture mode in south central Chile. J. Geophys. Res., Solid Earth 119 (3), 1607–1633.

Ramsey, C.B., 2008. Deposition models for chronological records. Quat. Sci. Rev. 27 (1–2), 42–60.

Reilinger, R., McClusky, S., Vernant, P., Lawrence, S., Ergintav, S., Cakmak, R., Ozener, H., Kadirov, F., Guliev, I., Stepanyan, R., Nadariya, M., 2006. GPS constraints on continental deformation in the Africa-Arabia-Eurasia continental collision zone and implications for the dynamics of plate interactions. J. Geophys. Res., Solid Earth 111 (B5).

Schmittbuhl, J., Karabulut, H., Lengliné, O., Bouchon, M., 2016. Long-lasting seismic repeaters in the Central Basin of the Main Marmara Fault. Geophys. Res. Lett. 43 (18), 9527–9534.

Şentürk, S., Çakır, Z., Ergintav, S., Karabulut, H., 2019. Reactivation of the Adıyaman Fault (Turkey) through the Mw 5.7 2007 Sivrice earthquake: an oblique listric normal faulting within the Arabian-Anatolian plate boundary observed by In-SAR. J. Geodyn. 131, 101654.

Strasser, M., Monecke, K., Schnellmann, M., Anselmetti, F.S., 2013. Lake sediments as natural seismographs: a compiled record of Late Quaternary earthquakes in Central Switzerland and its implication for Alpine deformation. Sedimentology 60 (1), 319–341.

Tan, O., Tapirdamaz, M.C., Yörük, A., 2008. The earthquake catalogues for Turkey. Turk. J. Earth Sci. 17 (2), 405–418.

Turkelli, N., Sandvol, E., Zor, E., Gok, R., Bekler, T., Al-Lazki, A., Bayraktutan, S., et al., 2003. Seismogenic zones in eastern Turkey. Geophys. Res. Lett. 30 (24).

Türkoğlu, E., Unsworth, M., Bulut, F., Çağlar, İ., 2015. Crustal structure of the North Anatolian and East Anatolian Fault Systems from magnetotelluric data. Phys. Earth Planet. Inter. 241, 1–14.

Van Daele, M., et al., 2015. A comparison of the sedimentary records of the 1960 and 2010 great Chilean earthquakes in 17 lakes: implications for quantitative lacustrine palaeoseismology. Sedimentology 62 (5), 1466–1496.

Yönlü, Ö., Altunel, E., Karabacak, V., 2017. Geological and geomorphological evidence for the southwestern extension of the East Anatolian Fault Zone, Turkey. Earth Planet. Sci. Lett. 469, 1–14.

Zor, E., Gürbüz, C., Türkelli, N., Sandvol, E., Seber, D., Barazangi, M., 2003. The crustal structure of the East Anatolian Plateau from receiver functions. Geophys. Res. Lett. 30 (24), 8044.